HD-sEMG-Based Control Using Neck Muscles and Shallow Neural Networks: Assessing Performance in Rehabilitation-Oriented Tasks

HD-sEMG-Based Control Using Neck Muscles and Shallow Neural Networks: Assessing Performance in Rehabilitation-Oriented Tasks

Giovanni Rolandino, Vinicius Taboni Lisboa, Taian Vieira, Alberto Cliquet Jr., Brian Andrews, and James J. FitzGerald, *Member, IEEE*

***Abstract*— This paper investigated the suitability of the integrated Recursive Rehabilitation Control Network (RRC-Net)/High-Density Electrode Array (HDE-Array) system for performing two multi-Degree of Freedom (DoF) control tasks, developed as proxies for Functional Electrical Stimulation control: 1) a cursor-based task; and 2) a 3-DoF hand kinematic model control task. The goal of this study is enhancing rehabilitation independence for individuals with spinal cord injuries. The system was validated on both healthy and tetraplegic subjects. The hypotheses that users could successfully perform these tasks using the system and that there would be no significant performance differences between healthy and tetraplegic participants were assessed. The experiment involved 10 tetraplegic and 8 healthy subjects who completed a training phase followed by two testing phases. High-Density surface Electromyography (HD-sEMG) signals recorded from the neck during the training phase were used to train RRC-Net, a neural network designed to estimate multi-DoF movements. Subjects then performed the two control tasks in the testing phase, and performance metrics were analysed and compared between groups. Healthy and tetraplegic subjects achieved high performance in both control tasks. Hand position control performance between the two groups presented no statistically significant differences in Mean Global Distance (MGD) (p = 0.93) or Mean Angular Distance (MAD) (p = 0.77). Similarly, cursor control task performance showed no significant differences in Task Completion Score (TCS) (p = 0.68) or Normalised Distance (ND) (p = 0.63). The system's simplicity, comfort, and effectiveness highlight its potential for rehabilitation, providing a non-invasive method for controlling assistive devices.**

***Index Terms*— Artificial neural networks, electromyography, machine learning.**

I. Introduction

CERVICAL-LEVEL Spinal Cord Injuries (SCIs), which often result in the loss of upper limb function, were reported at a rate of 10.7 per 100,000 individuals in the High-Income super region as of 2020 [1], [2], [3]. Functional Electrical Stimulation (FES), first developed in the 1960s, is a well-established technique that uses electrical stimuli to induce muscle contractions, enabling controlled limb movements with numerous applications for restoring upper limb functionality [4], [5], [6], [7]. Depending on the degree and phase of impairment, FES can be employed as a therapeutic intervention, as temporary support during rehabilitation, or as a permanent replacement for lost motor functions through assistive devices known as neuroprostheses [4], [8], [9], [10], [11], [12]. Despite substantial advances in FES and other rehabilitation technologies, progress in control solutions has lagged behind developments in actuation and hardware [11], [13], [14], [15], [16], [17], [18], [19], [20], [21]. Achieving user independence requires control strategies that minimise external assistance and exploit residual voluntary muscle activity, such as that available in the neck or shoulder region, depending on lesion level [22], [23].

Surface electromyography (sEMG) represents a promising solution, enabling intuitive, real-time control by leveraging signals from spared musculature. This is particularly relevant for individuals with high-level SCIs, as key neck muscles are innervated by cranial nerves and remain accessible even in very rostral lesions. Recent studies have investigated neck-derived sEMG as a control signal for assistive and rehabilitative applications, including robotic manipulators, adaptive recreational devices, and assistive neck exoskeletons in individuals with cervical spinal cord injury [24], [25], [26], [27]. Many of these approaches employ machine-learning-based decoding to improve robustness and real-time responsiveness, alongside efforts to develop wearable and user-friendly acquisition hardware [28]. Collectively, these studies demonstrate that neck sEMG constitutes a viable and intuitive control source for a range of assistive applications, supporting its use as an alternative to traditional limb-based interfaces when upper-limb function is compromised. Despite these advances,

Received 31 July 2025; revised 5 January 2026; accepted 10 February 2026. Date of publication 19 February 2026; date of current version 26 February 2026. Associate Editor: Dingguo Zhang. This work was supported by the John Fell Oxford University Press Research Fund under Grant 0014150. The work of James J. FitzGerald was supported by the National Institute of Health and Care Research Oxford Biomedical Research Centre. *(Corresponding author: Giovanni Rolandino.)*

This work involved human subjects or animals in its research. Approval of all ethical and experimental procedures and protocols was granted by the Research Ethics Committee at the State University of Campinas (CEP-UNICAMP) under Approval No. 34583120.2.0000.5404, and performed in line with the Declaration of Helsinki.

Giovanni Rolandino, Brian Andrews, and James J. FitzGerald are with the Nuffield Department of Surgical Sciences, University of Oxford, OX3 9DU Oxford, U.K. (e-mail: giovanni.rolandino@nds.ox.ac.uk).

Vinicius Taboni Lisboa and Alberto Cliquet Jr. are with the Department of Orthopedics, Rheumatology and Traumatology, University of Campinas, Campinas, São Paulo 13083-888, Brazil.

Taian Vieira is with LISiN, Department of Electronics and Telecommunications, Politecnico di Torino, 10129 Turin, Italy (e-mail: taian.martins@polito.it).

Data is available on-line at https://zenodo.org/records/14246378

Digital Object Identifier 10.1109/TNSRE.2026.3666280

sEMG-based rehabilitation systems often rely on outdated acquisition hardware or simplified control paradigms, and are typically validated using low-complexity tasks such as Fitts' law, rather than continuous multi-DoF motor control [29], [30], [31]. These limitations hinder usability and real-world applicability, highlighting the need for solutions that combine robust decoding, wearable high-quality EMG acquisition, and validation in tasks reflecting realistic multi-DoF control demands.

To address these challenges in EMG-driven control systems, a solution based on High-Density surface Electromyography (HD-sEMG) signals acquired from the forearm of healthy subjects was previously developed and validated: the Recursive Prosthetic Control Network (RPC-Net) combined with a High-Density Electrode Array (HDE-Array) [32], [33]. Although originally conceived for upper-limb prosthetic control, this system addresses many of the same methodological limitations encountered in the rehabilitation of upper limb impairment. Both domains require intuitive, robust, and responsive user interfaces for real-time motor control, and face common challenges, including limitations in EMG acquisition hardware, real-time performance constraints, and user comfort. The software component, RPC-Net, was designed to mitigate common shortcomings of EMG-based control algorithms, such as instability during online operation and sensitivity to signal variability, while HDE-Array enhances wearability and signal consistency, improving the overall practicality of EMG acquisition. Subsequent studies demonstrated the system's reliability in real-time use, robustness to electrode displacement and changes in skin condition, and compatibility with simplified kinematic models [34], [35], [36]. Building on the demonstrated effectiveness of the RPC-Net/HDE-Array system for upper-limb kinematic estimation using residual forearm muscle activity, and motivated by the growing evidence supporting neck muscles as a viable control source, this study investigates the applicability of the same framework when driven by neck-derived sEMG signals. By transferring the control paradigm from forearm to cervical musculature, the present work aims to address key limitations of EMG-based control in rehabilitation contexts where forearm muscles are unavailable or unreliable, such as in individuals with high-level cervical spinal cord injury.

The overarching goal of this study is to develop a comfortable, efficient, and cost-effective control framework for upper-limb rehabilitation devices in individuals with cervical spinal cord injury, where reliable and intuitive control interfaces remain a major clinical challenge, although the proposed framework may be applicable to a range of assistive technologies. To this end, the suitability of the integrated RPC-Net/HDE-Array system was evaluated using two multi-DoF control tasks designed to assess real-time kinematic control capabilities. These tasks were selected as proxies for control requirements relevant to complex rehabilitation devices, including multi-site FES systems, without directly implementing stimulation in the experimental protocol. The tasks were performed by both healthy and tetraplegic participants, enabling direct comparison of control performance between populations. This comparison serves to validate the proposed control strategy in the intended clinical population and to assess whether neck musculature remains a viable control source at the impairment levels considered (lesions caudal to C4), using unimpaired subjects as a reference. This is particularly relevant given that some neck muscles, such as the scalenes, receive cervical innervation and may be differentially affected by lesion level. Guided by these aims, the study tests the following hypotheses:

1) Subjects can control a hand kinematic model in real time using neck muscles and the RRC-Net/HDE-Array system, achieving task performance comparable to that observed with forearm muscle control
2) Performance in controlling the hand kinematic model is comparable between tetraplegic and healthy subjects
3) Subjects can successfully use the RRC-Net/HDE-Array system to control three independent cursors in a task-oriented experiment
4) Performance in the cursor-based task is comparable between healthy and tetraplegic subjects

Demonstrating this system's potential for intuitive multi-DoF control could contribute a practical and scalable solution for both short-term therapeutic use and long-term rehabilitation applications. To test these hypotheses, a new dataset based on the two tasks was acquired and compared against data from a previous study.

II. Materials and Methods

This section details the instrumentation and software used in the study (Section II-A), as well as the experimental procedures implemented to evaluate the stated hypotheses (Section II-B). All procedures were conducted in accordance with the Declaration of Helsinki and approved by the local ethics committee (CEP Unicamp, Approval Reference: 34583120.2.0000.5404). All data used in this study are available online [37].

A. Instrumentation

1) EMG Amplifier: EMG was recorded using the MEACS system, the EMG amplifier developed at LISiN (Politecnico di Torino, Turin, Italy) [38], [39]. The system is made up of multiple Sensor Units (SUs), each measuring 34 mm $\times$30 mm $\times$15 mm and sampling 32 channels at f_s = 2.048 kHz (192 V/V gain, 16-bit resolution, 2.4 V dynamic range). In this instance, two SUs were used, connected to the HDE-Array, the array of dry electrodes developed previously [33]. For neck application, the only modification in the HDE-Array configuration was adjustment of the embedded elastic band to ensure a secure but comfortable fit.

2) Acquisition Software: EMG data were acquired using the MEACS system with BP, a proprietary desktop application. The MEACS system streams raw EMG signals wirelessly to a laboratory desktop computer, where the BP application records, displays and processes them in real time. Subsequent data processing, including filtering and feature extraction, was performed in MATLAB (R2024a, The MathWorks, Inc.), and custom algorithms were implemented in Python using BSD-, BSD-Style- or MIT- licensed libraries (numpy, scipy, matplotlib, pyserial, torch, pyqtgraph, tqdm).

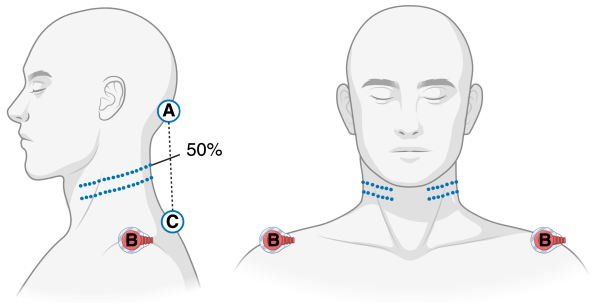

Fig. 1. **Electrode placement:** HDE-Array placement around the neck, showing the front and side views. Blue dots represent electrode locations. The array is positioned at 50% of the distance between the vertebra prominens (C) and the inion (A).

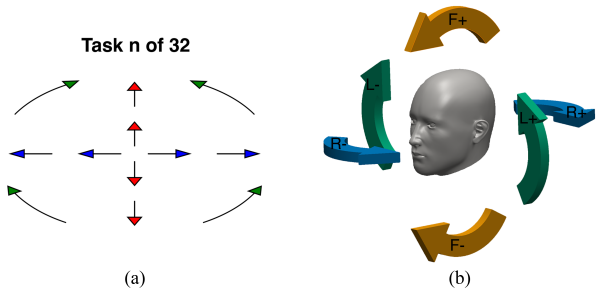

Fig. 2. **Directions of movement and corresponding labels** (a) Overlap of visual prompts shown in the Training Phase: at most two arrows were shown at a time, indicating only one direction and sense. Two arrows were used to indicate higher movement intensity, rather than varying arrow length, in order to improve visual readability and avoid ambiguity in the on-screen cue. (b) Directions of movement. F: neck flexion/extension (sagittal plane); L: neck lateral flexion (coronal plane); R: neck rotation (transverse plane). Flexion, right lateral flexion, right rotation are indicated by a + sign; extension, left lateral flexion, left rotation are indicated by a - sign.

B. Experimental Protocol

The objective of the experiments was to assess the hypotheses defined in Section I. The following subsections detail the data acquisition protocol, preprocessing pipeline, network training strategy, testing methodology, and performance evaluation metrics for the Recursive Rehabilitation Control Network (RRC-Net).

1) Data: Two datasets were used in this study, labelled as DS1 and DS2 [37]. DS1 was acquired for previous studies, while DS2 was acquired specifically for this study [35], [36]. For clarity and conciseness, the data collection and processing procedures used for DS2 are described in their entirety, while a summary only of the data acquisition procedure for DS1 is included. DS2 comprises three parts: a training phase (DS2.a) and two real-time testing phases (DS2.b.s1 and DS2.b.s2). DS2.a was used to train RRC-Net, while DS2.b.s1 and DS2.b.s2 include EMG data and corresponding RRC-Net real-time outputs recorded during a testing phase, enabling evaluation of the system under test conditions. A thorough description of DS1 acquisition procedures is provided in the relevant papers [35], [36].

2) DS2.a: Training Phase Data Acquisition: For the acquisition of this dataset, 10 tetraplegic (P1-P10) and 8 healthy participants (P11-P18) (age: 21-40 years; weight: 65-90 kg; height: 165-195 cm; neck circumference: 30-40 cm) were recruited. Data collection was conducted at the Department of Orthopaedics, Rheumatology, and Traumatology, State University of Campinas (SP, Brazil). All tetraplegic subjects had cervical spinal lesions at the C5 or C4-C5 level. Written informed consent was obtained from all participants. Each subject completed a single trial during the training phase. During this trial, HD-sEMG signals were recorded from the neck while subjects performed a sequence of motor tasks. Prior to recording, participants were seated, and the HDE-Array was positioned and connected to two MEACS SUs. The array, composed of 64 dry electrodes arranged in two circumferential rows, was placed around the neck with a gap over the trachea. The rostral row of electrodes was aligned at 50% of the distance between the inion and the vertebra prominens (points A and C in Figure 1). Reference electrodes were placed on the left and right acromia, one per Sensor Unit (SU) (point B in Figure 1).

The protocol included 13 distinct motor tasks, each defined by direction, sense, and magnitude.

- Direction was classified as: (1) F: neck flexion/extension (sagittal plane), (2) L: lateral flexion (coronal plane), and (3) R: rotation (transverse plane).
- Sense was labelled as positive (flexion, right lateral flexion, right rotation, indicated with a + sign) or negative (extension, left lateral flexion, left rotation, indicated with a - sign).
- Magnitude was set to either 1 or 2.

An additional rest condition was also included as a baseline task. Each trial consisted of 32 tasks, with each combination of direction, sense, and magnitude presented twice and the rest task repeated eight times. The sequence was randomised. Visual prompts were displayed on a monitor, each lasting 15 seconds (see Figure 2). Participants indicated readiness before each prompt; execution began when confirmed. Idle periods between tasks lasted 1-10 seconds, resulting in total trial durations ranging from 8 to 12 minutes. The diversity of tasks enabled robust decoding across neck movement types. After the training trial, the HDE-Array remained in place for the subsequent testing phase while the HD-sEMG signals, together with task labels, were pre-processed and used to train RRC-Net on a per-subject basis.

3) HD-sEMG Pre-Processing and RRC-Net Training: Following the acquisition of training data, the objective of this procedure was to train RRC-Net to estimate continuous neck movement trajectories in the three anatomical directions defined in the experimental protocol, using HD-sEMG signals. Initial HD-sEMG preprocessing was conducted in real time using BP software. Raw signals were converted from bits to volts, offset-corrected, rectified, and transformed into Root Mean Square (RMS) values using a 307-sample (150 ms) sliding window with no overlap. The choice of the sliding window length was driven by instrumentation constraints. RMS features were computed and streamed by BP, the proprietary acquisition software, at its maximum supported update rate (6.8 Hz, corresponding to one update every 148 ms when using two sensor units). Shorter analysis windows would have required higher update rates than could be transmitted and processed reliably within the current hardware and software configuration. The data were temporarily cached and later used

for network training. RMS values were scaled by a factor of 10^4 to standardise input variance and mean. The resulting signals served as the input to RRC-Net during training. The training labels consisted of a three-element array, where each element represented the signed magnitude of movement in one of the three anatomical directions.

RRC-Net is a neural network designed to predict multi-dimensional movement states from neck-acquired HD-sEMG, building upon the earlier RPC-Net model for hand kinematic estimation [32]. At each inference step, RRC-Net processes the eight most recent samples from 64 EMG channels, producing a 512-dimensional input vector. The network architecture comprises six fully connected layers with 512, 1024, 2048, 1024, 512, and 3 neurons, respectively. All layers use ReLU activation functions, except for the output layer, which generates three continuous outputs corresponding to the three movement directions, with values ranging from -2 to 2, through a scaled sigmoid activation function. The objective of the training phase was to minimise the mean squared error between the output of RRC-Net and the target label vectors included in the dataset. The training dataset (DS2.a) was split 90/10 for training and validation. RRC-Net was trained independently for each subject using 100 epochs, with the Adam optimiser (learning rate 10^{-12}, $\varepsilon = 10^{-5}$, $\beta_1 = 0.9$, $\beta_2 = 0.99$, batch size = 400) and a mean squared error loss function, all implemented in PyTorch. The selection of optimisation hyperparameters was carried out through a preliminary tuning phase on a separate dataset, during which candidate values were evaluated and iteratively refined. Final values were chosen based on stable convergence behaviour (i.e., absence of divergence or overfitting) and performance plateauing within a short training time, consistent with standard procedures for subject-specific model training. RRC-Net's average inference time was 250 μs ($\pm$22 μs), measured across 10^5 iterations on an Intel(R) Xeon(R) Platinum 8268 Central Processing Unit (2.90 GHz). Training time per subject was approximately five minutes. The trained network was subsequently used in the testing phase.

4) DS2.b.s1: Testing Phase Data Acquisition Part 1: The testing phase began immediately after RRC-Net training and resulted in the acquisition of DS2.b. This phase was divided into two parts: cursor control (DS2.b.s1) and hand control (DS2.b.s2). Throughout testing, subjects remained seated in the same position used during training, and the HDE-Array was not repositioned. Both parts of the testing phase were completed by each subject in a single continuous session, using the same experimental setup and electrode placement. In Part 1 (DS2.b.s1), subjects controlled three on-screen cursors in real time via neck muscle activation and RRC-Net, with each cursor corresponding to one of the three movement directions. HD-sEMG signals were streamed through the MEACS system and processed in real time by the BP software, which computed RMS values using a 307-sample (150 ms) sliding window updated every 150 ms. These RMS values were passed to a Python-based application running RRC-Net, which converted them into control signals for the visual interface. The system operated at a refresh rate of 6 frames per second.

Visual tasks were presented alongside the cursors on a monitor. Cursors and task lines were colour-coded by direction using the same scheme as in the training phase (Figure 2). Each task involved a target and a constraint requirement. Continuous lines (targets) indicated that the subject needed to push the corresponding cursor beyond a fixed magnitude (set at 1.5). Dashed lines (thresholds), set at a magnitude of 0.5, required the subject to keep the associated cursor below that level. Subjects performed seven distinct task types. The first (N) required maintaining all three cursors below their thresholds. The remaining six (R+, R-, F+, F-, L+, L-) each focused on one movement direction as the target, with the other two directions acting as constraints (see Figure 3). Each task was performed twice, resulting in a total of 14 trials. Tasks were performed at the participants' own pace, advancing to the next upon completion. The average duration of a prompt was 13.4 s ($\pm$ 10.6 s). Each task was classified according to performance:

- failed, if the target was not reached;
- partially completed, if the target was reached but constraint thresholds were violated;
- completed, if the target was reached while staying below both thresholds.

For the rest task (N), outcomes were classified as either completed or failed, since no target was involved (see Figure 3 for examples). In addition to categorical outcomes, the distance between the target line and the corresponding cursor was recorded as a continuous measure of task success.

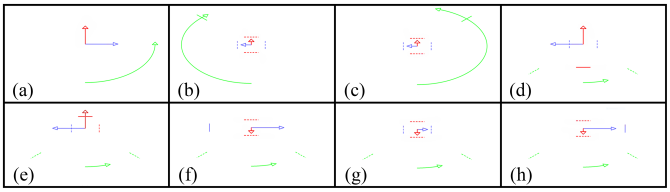

Fig. 3. **Tasks prompted during the first part of the testing phase:** Visual tasks were presented alongside the cursors on a monitor. Cursors and task lines were colour-coded by direction using the same scheme as in the training phase. Each task involved a target and a constraint requirement. Continuous lines (targets) indicated that the subject needed to push the corresponding cursor beyond a fixed magnitude (set at 1.5). Dashed lines (thresholds), set at a magnitude of 0.5, required the subject to keep the associated cursor below that level. (a) No task displayed. (b) "L+", Positive lateral flexion task, subject successfully reached the target while remaining below threshold for the two other directions. (c) "L-", Negative lateral flexion task, subject successfully reached the target while remaining below threshold for the two other directions. (d) "F+", Positive flexion task, subject did not reach the target and failed to stay below threshold for the other two directions. (e) "F-", Negative flexion task, subject reached the target but failed to stay below threshold for the other two directions. (f) "R-" Negative rotation task, subject failed to reach the target but stayed below threshold for the other two directions. (g) Rest task, subject successfully stayed below threshold for all directions. (h) "R+", Positive rotation task, subject failed to reach the target but stayed below threshold for the other two directions.

5) DS2.b.s2: Testing Phase Data Acquisition Part 2: In Part 2 (DS2.b.s2), participants used RRC-Net to control a virtual 3-Degree of Freedom (DoF) hand kinematic model. The acquisition, transmission, and processing of HD-sEMG data were identical to those in Part 1. However, instead of moving visual cursors, the three outputs of the RRC-Net model were mapped to control a virtual hand in 3-dimensional (3D) space.

This mapping was based on results from a previous study in which Principal Component Analysis (PCA) was applied to

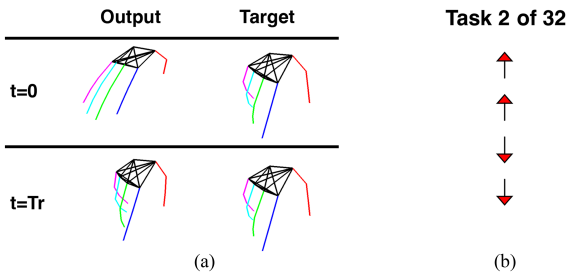

Fig. 4. **Testing phase part 2 example:** (a) The left part of the plot shows the prompted task (Target) and the initial output configuration. After the subject was given time to reach the target (time T_r), the two configurations were similar. (b) The second window displays the direction of movement but not its sense.

a 29-DoF hand kinematic model [34]. The first three Principal Components (PCs) captured 60% of the total variance. The three outputs of RRC-Net were projected onto these three PCs using precomputed PCA coefficients. From the resulting three-dimensional representation, the full 29-DoF joint configuration was reconstructed through inverse PCA and passed through a Forward Kinematic Algorithm (FKA) to compute and render the hand's position in space. To improve stability and control precision, the outputs were scaled down by a factor of two. Each neck movement direction was associated with one of the three PCs: axial rotation controlled PC1, flexion/extension controlled PC2, and lateral flexion controlled PC3. The resulting output was a virtual hand displayed on the monitor in front of the participant.

As in Part 1, participants completed control tasks by imitating a visual prompt. Three elements were simultaneously shown on the display:

- the target hand configuration, displayed as a skeletal hand model (Figure 4.a),
- the live output of the RRC-Net model, also rendered as a skeletal hand (Figure 4.a),
- a directional cue indicating the suggested direction of movement, presented as unlabelled arrows (Figure 4.b).

Upon appearance of the prompt, participants were instructed to imitate the target pose using the live output as accurately as possible. Seven task types were defined, each corresponding to a specific prompt. The first task (N) represented a rest condition with no Principal Component (PC) activation. The remaining six tasks (M1-M6) involved isolated activation of a single PC (positive or negative) with a magnitude of 0.75, while the other two PCs remained at zero. The hand configurations associated with each task are illustrated in Figure 5. Tasks involving opposite directions along the same PC axis were paired (PC1: M1, M4; PC2: M2, M5; PC3: M3, M6), with the rest pose centred among them. Each task type was presented twice during a session, resulting in a total of 14 prompts. A new prompt appeared upon the participant's request, and they were allowed to take as much time as needed to match the target pose. The average duration per prompt was 13.6 s ($\pm$ 10.0 s). Task performance was quantified based on the distance between the target and actual hand configurations, rather than using binary success/failure criteria.

6) DS1: Data From Previous Study: Hand Position Control via Forearm Muscles: Evaluation of the first experimental hypothesis used previously recorded HD-sEMG and kinematic

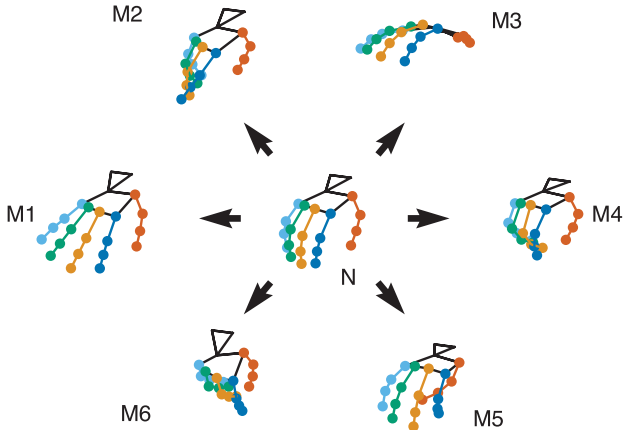

Fig. 5. **Hand control tasks:** The figure displays the seven tasks performed by subjects in terms of control of a virtual hand kinematic model. Tasks involving activation of the same PC in opposite directions are aligned along the same axis: PC1 (M1 and M4), PC2 (M2 and M5), and PC3 (M3 and M6). Rest state (N) is centred between them.

data as a benchmark. These data were acquired in a prior study, where the ability of subjects to control a virtual hand kinematic model using proximal forearm muscles through RPC-Net was assessed [36]. This dataset is referred to as DS1 throughout this paper. DS1 consists of two subsets, DS1.a and DS1.b. For the purposes of the present study, only DS1.b was used. It includes recordings from four subjects who performed six hand control tasks similar to those in Part 2 of the current testing phase. The aim was to compare the effectiveness of virtual hand control using forearm-acquired signals with results obtained from neck-based control in the present study. Full methodological and technical details of DS1 are provided in the relevant paper [36].

7) Performance Assessment: To assess both subject performance and the effectiveness of the RRC-Net/HDE-Array system, different performance metrics were used for Part 1 and Part 2 of the testing phase.

For Part 1, performance was evaluated using two metrics: Task Completion Score (TCS) and Normalised Distance (ND). Because Part 1 tasks involved simultaneous target-reaching and constraint-avoidance, simple and complex evaluation metrics were defined to capture different levels of task success. TCS is defined as the ratio of successfully completed tasks to the total number of tasks, with values ranging from 0 to 1. Higher TCS values indicate better performance.

Two variations of TCS were calculated:

- TCS-Simple (TCS-S): the fraction of tasks that were either completed or partially completed.
- TCS-Complex (TCS-C): the fraction of tasks that were fully completed (i.e., target reached and constraints satisfied).

ND quantifies the spatial closeness between the active cursor and its target in each task. Lower ND values indicate better performance. The following are defined:

- ND-Simple (ND-S): minimum distance between the active cursor and its target line, divided by 1.5.
- ND-Complex (ND-C): calculated as ND-S, but only during time periods when the other two movement directions remained below their respective thresholds.

For the rest task (N), where no active target was present, TCS-S and TCS-C were identical. In this case, ND was computed as the mean minimum distance of all three cursors from zero. All TCS and ND values were averaged across subjects and tasks. Distance and output signals were smoothed using a moving average with a 1.5 s window before metric computation.

For Part 2, performance was evaluated using two metrics: Mean Angular Distance (MAD) and Mean Global Distance (MGD). Both quantify the deviation between the reconstructed hand output and the target pose, with lower values indicating better performance. MAD quantifies joint-space angular error across the 29 degrees of freedom, whereas MGD evaluates spatial accuracy in task space by measuring the 3D discrepancy between reconstructed and target hand configurations after forward kinematics. The two metrics capture complementary aspects of control: while MAD reflects angular precision, joint-space errors are not directly comparable across joints and small proximal deviations can lead to large distal displacements. MGD therefore provides a more intuitive measure of overall hand-shape and end-effector accuracy. Reporting both metrics also enables direct comparison with our previous forearm-based studies, where the same measures were used [36].

MAD measures the joint-space angular error. At each time step, the absolute difference between the 29 reconstructed joint angles from RRC-Net and the target angles was computed. Target joint angles were derived by applying inverse PCA (with the same coefficients as used during training) to a task activation signal defined as a unit-magnitude step on the relevant principal component. The resulting time series of differences (signal A) was smoothed using a 1.5 s moving average (yielding signal B), and the minimum value of B over the task duration was recorded as the MAD for each subject-task pair. MGD captures spatial accuracy by comparing full 3D hand poses. At each time point, RRC-Net's 29 output angles were converted to 3D hand positions using the FKA defined in a previous study, producing a set of 20 spatial points [33]. The same transformation was applied to target angles. The Euclidean distances between estimated and target hand position points were computed over time and averaged into a time-varying signal (A). A moving average (1.5 s window) was applied to obtain the smoothed signal (B). For each task, the minimum value of B was recorded as the MGD for the corresponding subject-task combination.

MAD and MGD values were also computed for the DS1.b dataset to provide a benchmark for comparison. In DS1.b, four subjects performed six hand control tasks using forearm-based control. For each subject, the mean MAD and MGD values were computed across all tasks. The mean, maximum, and minimum values across subjects are reported in the results section.

8) Hypotheses Testing: Four hypotheses were tested to evaluate performance of the RRC-Net/HDE-Array system in enabling control of either on-screen cursors or a virtual hand model using neck muscle activation.

1) Subjects can control a hand kinematic model in real time using neck muscles and the RRC-Net/HDE-Array system, achieving task performance comparable to that observed with forearm muscle control: to assess this, MAD and MGD values from Part 2 of the testing phase were compared with those obtained from the forearm-based dataset (DS1.b) [36]. Values from this study were grouped by task (M1-M6 and N), yielding 8 or 10 data points per task depending on group size (8 tetraplegic, 10 healthy subjects). These values were plotted alongside the mean across subjects for each task. In addition, MAD and MGD values were grouped by subject, and both task-wise and subject-wise means were visualised. A descriptive comparison was conducted to assess relative performance across control modalities.
2) Performance in controlling the hand kinematic model is comparable between tetraplegic and healthy subjects: Unpaired t-tests on MAD and MGD values from Part 2 were conducted to evaluate this. Each data point represented a subject's mean performance across all tasks. The null hypothesis (H_0) assumed equal means between groups. Prior to testing, normality was assessed using the Shapiro-Wilk test.
3) Subjects can successfully use the RRC-Net/HDE-Array system to control three independent cursors in a task-oriented experiment: This hypothesis was evaluated qualitatively based on aggregate performance scores in Part 1 and visual inspection of TCS and ND metrics. System usability and subject response patterns were assessed descriptively, and outcomes were compared to performance ranges reported in related studies using sEMG-driven cursor control.
4) Performance in the cursor-based task is comparable between healthy and tetraplegic subjects: Group differences in cursor-based task performance were assessed using a Mann-Whitney U test for TCS-S and TCS-C values, as normality assumptions were not met (Shapiro-Wilk test). For ND-S and ND-C values, normality was satisfied and an unpaired t-test was used. In both cases, each data point represented a subject's mean score across all tasks. The null hypotheses assumed equal distributions for the Mann-Whitney U test and equal means for the t-test.

These hypotheses formed the basis for evaluating both usability and efficacy of the RRC-Net/HDE-Array system across subject populations and task types.

III. Results

This section presents the findings from the assessments described in Section II-B8. Control performance between tetraplegic and healthy subjects is compared for both cursor and hand position control. Additionally, hand position control using forearm- and neck-based approaches is contrasted, and feasibility of cursor control tasks with the RRC-Net/HDE-Array system is assessed.

A. Assessment of Hand Control Performance

Figure 6 shows the values of MGD and MAD for the 18 subjects considered. The plots in the left column present data grouped by task, with black point markers representing

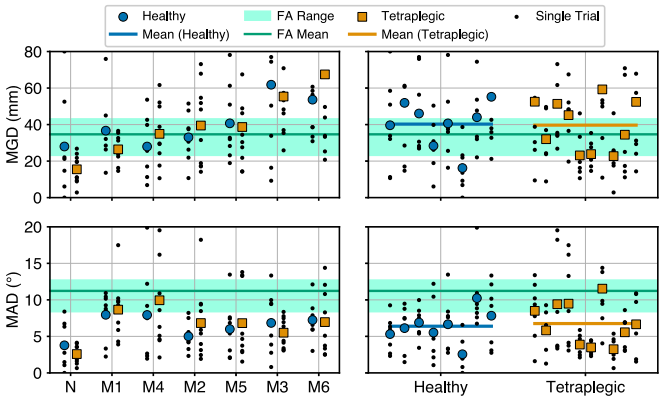

Fig. 6. **Hand Control Task Performance Results:** This figure shows the results, in terms of MGD and MAD, of the experiment assessing the ability of healthy and tetraplegic subjects to control a virtual hand model. (Left) data are grouped by task, as indicated on the *x*-axis. (Right) data are grouped by subject type (healthy or tetraplegic). Unpaired t-test results for MGD (H_0: $\mu_T = \mu_H$): $t(16) = 0.09$, $p = 9.3 \cdot 10^{-1}$). Unpaired t-test results for MAD (H_0: $\mu_T = \mu_H$): $t(16) = -0.30$, $p = 7.7 \cdot 10^{-1}$).

TABLE I
CURSOR CONTROL RESULTS

	MGD		MAD	
Task	Healthy	Tetraplegic	Healthy	Tetraplegic
M1	36.7 mm	26.4 mm	8°	9°
M2	33.0 mm	39.5 mm	5°	7°
M3	61.8 mm	55.3 mm	7°	6°
M4	28.0 mm	34.9 mm	8°	10°
M5	40.7 mm	38.7 mm	6°	7°
M6	53.7 mm	67.4 mm	7°	7°
N	28.0 mm	15.5 mm	4°	3°
Mean	40.2 mm	39.7 mm	6°	7°

Forearm Baseline		
Min	23.1 mm	8°
Mean	34.7 mm	11°
Max	43.1 mm	13°

Performance of RRC-Net across tasks for both populations (hand control). Mean MGD and MAD values are shown. Minimum, mean, and maximum values from DS1.b are also included.

individual trials. Square and circular markers indicate the group average for each task. The plots in the right column group individual trials by subject and include the group-wide mean. Additionally, a green line represents the average observed across the four subjects in the study using forearm muscles as the control source (i.e., from DS1.b). The shaded area represents the range (maximum and minimum) observed in DS1.b. Because tasks differed between the two studies, no task-wise distinction was made. For MGD, the mean values observed in both populations (Healthy: 40.2 mm, Tetraplegic: 39.7 mm) fall within the range reported in the previous study (23.1 mm-43.1 mm) and deviate by less than 8 mm from its mean (34.7 mm) in both cases. At the level of individual tasks and subjects, all tasks except M3 and M6 fell within or below this range, and approximately half of subjects in both populations displayed average performance within the reference range. In contrast, results for MAD were notably different. In this case, the mean for both populations (Healthy: 6°, Tetraplegic: 7°) is not only below the mean observed in the previous study (11°) but also outside its reported range (8°-13°). Specifically, only tasks M1 and M4 fall within the reference range, and approximately one-third of the subjects

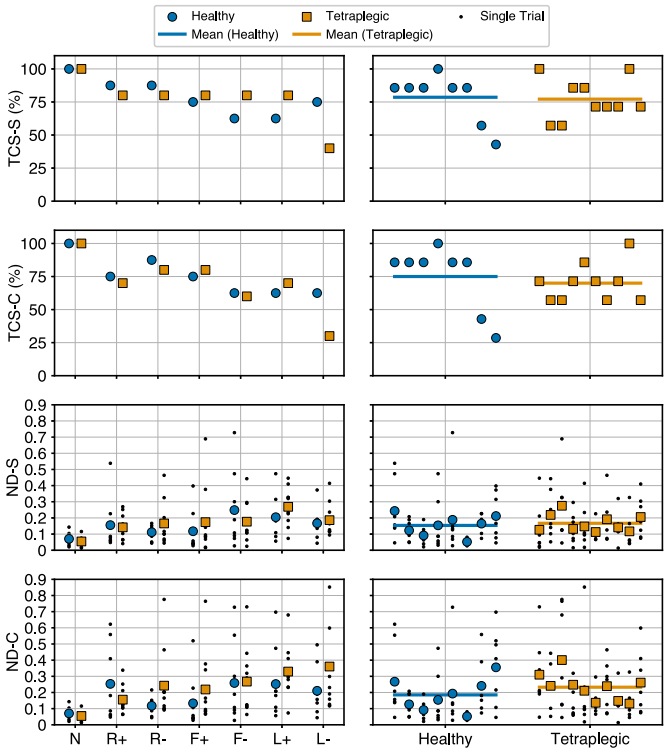

Fig. 7. **Cursor Control Task Performance Results:** This figure shows the results, in terms of TCS-S, TCS-C, ND-S and ND-C, of the experiment assessing the ability of healthy and tetraplegic subjects to control three independent cursors. (Left) data are grouped by task, as indicated on the *x*-axis. (Right) data are grouped by subject type (healthy or tetraplegic). Mann-Whitney U test results for TCS-S (H_0: P(H ≥ T) = P(T ≥ H)): $U = 45$, $p = 6.8 \cdot 10^{-1}$. Mann-Whitney U test results for TCS-C (H_0: P(H ≥ T) = P(T ≥ H)): $U = 52$, $p = 2.9 \cdot 10^{-1}$. Unpaired t-test results for ND-S (H_0: $\mu_T = \mu_H$): $t(16) = -0.48$, $p = 6.4 \cdot 10^{-1}$). Unpaired t-test results for ND-C (H_0: $\mu_T = \mu_H$): $t(16) = -1.10$, $p = 2.9 \cdot 10^{-1}$).

show values within this interval. A summary of the results from this experiment is provided in Table I.

B. Healthy Vs. Tetraplegic Subjects: Hand Position Control

Figure 6 presents the comparison of virtual hand position control performance between healthy and tetraplegic subjects using neck muscles. The mean MGD for healthy subjects was 40.2 mm (range: 28.0 mm-61.8 mm), while for tetraplegic subjects, it was 39.7 mm (range: 15.5 mm-55.3 mm). An unpaired t-test was conducted to assess whether mean values differed between the two groups under the null hypothesis (H_0) of equal means. The test yielded a p-value of 0.93 for MGD and 0.77 for MAD, indicating no statistically significant difference between the groups for either metric. The numerical results are detailed in Table I.

C. Assessment of Cursor Control Performance

Figure 7 presents the results of the experiment assessing subjects' ability to control a cursor on the screen using neck muscles. The figure reports values for TCS-S, TCS-C, ND-S, and ND-C across tasks and subjects. The corresponding numerical results are detailed in Table II. Results indicated that TCS-S exceeded 50% for all but one task and reached or surpassed 75% in four of the seven tasks. Performance

TABLE II
HAND POSITION ESTIMATION RESULTS

Task	TCS (%)				ND			
	S		C		S		C	
	H	T	H	T	H	T	H	T
R+	87.5	80	75	70	0.16	0.14	0.25	0.16
R-	87.5	80	87.5	80	0.11	0.17	0.12	0.24
F+	75	80	75	80	0.12	0.17	0.13	0.22
F-	62.5	80	62.5	60	0.25	0.18	0.26	0.27
L+	62.5	80	62.5	70	0.20	0.27	0.25	0.33
L-	75	40	62.5	30	0.17	0.19	0.21	0.36
N	100	100	100	100	0.07	0.05	0.07	0.05
Mean	78.6	77.2	75	70	0.15	0.17	0.19	0.23

Performance of RRC-Net across tasks for both populations (cursor control). Mean ND-S, ND-C, TCS-S, and TCS-C values are shown. Columns "H" and "T" represent healthy and tetraplegic subjects, respectively.

was lower for tasks F and L, while the N task consistently achieved a perfect score. The distribution of values across subjects was broad, with values evenly spread around the mean (77.8%). A similar pattern was observed for TCS-C, suggesting a uniform decline in performance rather than a pronounced drop in specific subjects or tasks. The mean TCS-C value is 72.2%, representing a 7% decrease from TCS-S. This indicated a modest decline in performance when subjects were also required to constrain movement in the other two directions. A Wilcoxon signed-rank test comparing the two metrics confirmed this difference (H_0: P(C $\geq$ S) = P(S $\geq$ C)), which yielded $W = 0$, $p = 2.7 \cdot 10^{-2}$.

For ND-S, similar trends were observed. Performance was highest in the rest task and progressively decreased across other tasks. The normalised distance remained below 0.4 for all tasks, indicating relatively high accuracy. For reference, the target was positioned at a distance of 1 from the centre of the dynamic range (after normalisation by 1.5), so a distance of 0.4 corresponded to achieving over 60% of the required movement. Regarding subject-wise distributions, values for ND-S were normally distributed around the mean, as confirmed by a Shapiro-Wilk test. A slight decrease in performance was observed for ND-C, aligning with trends seen in TCS. Mean ND-S and ND-C values were 0.16 and 0.21 respectively, indicating a 24% increase in normalised distance when subjects were also required to remain below thresholds for the other movement directions. Comparison of ND-S and ND-C values using a paired t-test (H_0: $\mu_S = \mu_C$) returned $t(17) = -3.79$ ($p = 1.5 \cdot 10^{-3}$), indicating a statistically significant difference between the metrics.

D. Healthy Vs. Tetraplegic Subjects: Cursor Control

Statistical tests assessed whether the four performance metrics differed significantly between the two populations. For TCS-S and TCS-C, a Mann-Whitney U test assessed differences under the null hypothesis (H_0) that both groups followed the same distribution. The test yielded p-values of 0.68 for TCS-S and 0.29 for TCS-C, indicating no statistically significant difference between the groups. For ND-S and ND-C, normality was confirmed by a Shapiro-Wilk test, allowing unpaired two-sided t-tests. The results returned p-values of 0.63 for ND-S and 0.29 for ND-C, again indicating no significant differences between the two populations.

IV. DISCUSSION

Results presented in the previous section demonstrate that neck muscles can effectively control a 3-DoF hand kinematic model or three independent cursors, with no significant performance difference between healthy and tetraplegic subjects (lesions at the C5 or C4-C5 level). This study aimed to validate four experimental hypotheses.

The first hypothesis, that subjects can control a hand kinematic model in real time using neck muscles and the RRC-Net/HDE-Array system with performance comparable to forearm-based control, was supported by the results in Section III-A. Mean MGD and MAD values generally fell within or below the performance range previously reported for forearm control [36]. Direct statistical comparison was not possible due to differences in experimental design, including sample size, task definitions, and the use of dimensionality reduction in the present study. Consequently, these similarities should be interpreted as indicative rather than conclusive. The lower MAD values observed here may partly reflect reduced task complexity, as control was limited to single principal components; the effect of increasing task dimensionality warrants further investigation. Interpretation of MGD requires care, as it is a task-space metric computed after forward kinematics and averaged across multiple hand points referenced from the wrist. As a result, small angular deviations distributed across several joints can accumulate into centimetre-scale spatial errors, particularly at distal segments and in the presence of proximal joint errors. MGD values should therefore not be interpreted as isolated finger displacements. Reporting both MAD and MGD is informative, as the two metrics capture complementary aspects of performance: MAD reflects joint-space accuracy, while MGD provides an intuitive spatial measure of overall kinematic reconstruction fidelity.

EEG-based decoding represents an alternative control modality for individuals with cervical spinal cord injury and has been increasingly explored for upper-limb movement estimation [40], [41]. However, direct comparison with the present results is limited by substantial differences in experimental paradigms and evaluation metrics. Many EEG studies focus on hand kinematics or classification-based decoding rather than continuous finger-level regression [42], [43], [44], [45], [46]. Although recent work has demonstrated continuous finger kinematic decoding from EEG, differences in metrics and protocols preclude quantitative comparison [47]. Systematic cross-modal comparisons between EEG- and EMG-based frameworks therefore remain an important topic for future research.

Previous studies have established the feasibility of neck-derived sEMG for assistive control, including multimodal interfaces for robotic manipulators in tetraplegia, classification-based control of powered neck exoskeletons, and low-dimensional continuous interfaces such as cursor or game control [25], [26], [27]. These approaches predominantly rely on sparse electrode configurations and discrete or low-dimensional control strategies. In contrast, the present work combines high-density sEMG acquisition with regression-based decoding to enable continuous multi-degree-of-freedom

kinematic control, evaluated using quantitative joint-space and task-space error metrics in both healthy and tetraplegic participants. This positions the proposed framework in a distinct control regime relevant to advanced upper-limb rehabilitation applications.

The second hypothesis proposed that performance in controlling a virtual hand kinematic model would not differ between healthy and tetraplegic subjects. The results support this hypothesis, as indicated by the high p-values from the unpaired two-sided t-tests (0.93 for MGD and 0.77 for MAD). While the results suggest slightly better MGD performance in the tetraplegic group (by 0.5 mm) and slightly better MAD performance in the healthy group (by 1°), these differences were not statistically significant. Analysis of individual task performance also supports this conclusion. Performance trends were consistent across both groups: tasks M3 and M6 had the highest MGD values (i.e., lowest spatial accuracy), and tasks M1 and M4 had the highest MAD values (i.e., largest angular deviations from target poses). Muscle fatigue is a potential consideration for neck-based control interfaces. Although fatigue was not quantitatively assessed, participants in both groups reported no noticeable discomfort, and no qualitative performance degradation was observed during the experiments. Fatigue effects may nonetheless emerge during longer sessions or real-world use, particularly in individuals with neuromuscular impairment, and should be investigated in future studies using longer protocols.

The third hypothesis stated that subjects could successfully use the RRC-Net/HDE-Array system to control three independent cursors in a task-oriented experiment. The findings support this hypothesis, as evidenced by high task completion rates (TCS-S and TCS-C) and low distances between cursor and target (ND-S and ND-C). A statistically significant but relatively small decrease in performance was observed between TCS-S and TCS-C, suggesting a modest reduction in the ability to precisely control one cursor while suppressing activation in the other two directions. Nonetheless, the small magnitude of this difference reinforces the feasibility of using neck muscles as a control source for managing three independent degrees of freedom. These findings indicate that such a system could serve as a viable and effective method for multidimensional control. These results align with prior work in the literature, which has also explored neck-based control, albeit with notable limitations, as a potential method for multidimensional interface manipulation [29], [30], [31].

Finally, the fourth hypothesis proposed that performance in the cursor-based task would not differ between the two populations. Results support this hypothesis, as indicated by high p-values from Mann-Whitney U tests for TCS-S (0.68) and TCS-C (0.29), showing no significant performance differences between healthy and tetraplegic subjects. Similar outcomes were observed for ND-S and ND-C, where unpaired t-tests yielded p-values of 0.63 and 0.29, respectively. Although tetraplegic subjects exhibited slightly lower performance on average, these differences were not statistically significant and did not affect conclusions drawn from the Mann-Whitney U tests. In conclusion, experimental results support the fourth hypothesis.

V. Conclusion

This study evaluated the ability of tetraplegic subjects with lesions at the C5 or C4-C5 level to perform control tasks using neck muscles as a control source, and compared their performance to that of healthy subjects and to previously reported tasks involving forearm muscle control. The results showed no significant differences between healthy and tetraplegic participants in either control paradigm. Furthermore, despite differences in experimental protocols, performance achieved using neck muscles was comparable to that obtained with forearm-based control. These findings, combined with the simplicity of the system (requiring less than 30 minutes of training) and its non-invasive nature, underscore the potential of the RRC-Net/HDE-Array system for tetraplegic rehabilitation. All tetraplegic participants reported the device as comfortable, further supporting its practical viability. The system could be adapted to control a three-site FES system from the neck, either for long-term assistive use or as a therapeutic training tool. It also holds potential for integration with other rehabilitation technologies, such as upper limb exoskeletons. Future studies are planned to validate the system's efficacy in controlling rehabilitation devices in real-time settings. The ability to intuitively and directly control a rehabilitation device could be transformative for individuals with cervical spinal cord injuries, offering greater autonomy and improved quality of life. Overall, the RRC-Net/HDE-Array system shows strong promise for expanding rehabilitation options and enhancing user experiences for the tetraplegic population.

Acknowledgment

The authors would like to thank the members of ONIG in Oxford and of the Department of Orthopedics, Rheumatology and Traumatology, University of Campinas. They also would like to acknowledge the use of the University of Oxford Advanced Research Computing (ARC) facility in carrying out this work [48]. Fig. 1 was created with BioRender.com.

References

[1] W. Ding et al., "Spinal cord injury: The global incidence, prevalence, and disability from the global burden of disease study 2019," *Spine*, vol. 47, no. 21, pp. 1532–1540, Nov. 2022.

[2] *SCIMS 2022 Annual Report-complete Public Version*, National Spinal Cord Injury Statistical Center, Birmingham, AL, USA, 2022.

[3] M. Fehlings, A. Singh, L. Tetreault, S. Kalsi-Ryan, and A. Nouri, "Global prevalence and incidence of traumatic spinal cord injury," *Clin. Epidemiology*, vol. 6, pp. 309–331, Sep. 2014.

[4] C. Marquez-Chin and M. R. Popovic, "Functional electrical stimulation therapy for restoration of motor function after spinal cord injury and stroke: A review," *Biomed. Eng. OnLine*, vol. 19, no. 1, p. 34, Dec. 2020.

[5] Y.-X. Wang and Z.-Z. Luo, "Research on the effect of mt+ fes training on sensorimotor cortex," *Neural Plasticity*, vol. 2022, no. 1, p. 6385755, 2022, Art. no. 6385755.

[6] J.-D. Yang et al., "Effectiveness of electrical stimulation therapy in improving arm function after stroke: A systematic review and a meta-analysis of randomised controlled trials," *Clin. Rehabil.*, vol. 33, no. 8, pp. 1286–1297, Aug. 2019.

[7] M. Sun et al., "Meta-analysis of functional electrical stimulation combined with occupational therapy on post-stroke limb functional recovery and quality of life," *Cerebrovascular Diseases*, vol. 53, no. 6, pp. 743–752, 2025.

[8] A. Ventura, J. M. P. Bataglia, G. Ginja, R. Varoto, and A. Cliquet, "Design and fast-fabrication of a system for functional electrical stimulation in upper limb of people with tetraplegia," *Spinal Cord Ser. Cases*, vol. 8, no. 1, p. 54, May 2022.

[9] M. Crepaldi et al., "FITFES: A wearable myoelectrically controlled functional electrical stimulator designed using a user-centered approach," *IEEE Trans. Neural Syst. Rehabil. Eng.*, vol. 29, pp. 2142–2152, 2021.

[10] P. Müller, A. J. del Ama, J. C. Moreno, and T. Schauer, "Adaptive multichannel FES neuroprosthesis with learning control and automatic gait assessment," *J. NeuroEngineering Rehabil.*, vol. 17, no. 1, pp. 1–20, Dec. 2020.

[11] D. B. Popović and L. Popović-Maneski, "Neuroprosthesis and functional electrical stimulation (peripheral)," in *Handbook of Neuroengineering*. Springer, 2022, pp. 1–40.

[12] M. Khantan et al., "The nurosleeve, a user-centered 3D printed orthosis and functional electrical stimulation system for individuals with upper extremity impairment," *J. NeuroEng. Rehabil.*, vol. 20, no. 103, Aug. 2023.

[13] J. Zhou, C. T. Freeman, and W. Holderbaum, "Multiple-model iterative learning control with application to stroke rehabilitation," *Control Eng. Pract.*, vol. 154, Jan. 2025, Art. no. 106134.

[14] M. Sun et al., "FES-UPP: A flexible functional electrical stimulation system to support upper limb functional activity practice," *Frontiers Neurosci.*, vol. 12, p. 449, Jul. 2018.

[15] C. Salchow-Hömmen et al., "User-centered practicability analysis of two identification strategies in electrode arrays for FES induced hand motion in early stroke rehabilitation," *J. NeuroEngineering Rehabil.*, vol. 15, no. 1, pp. 1–19, Dec. 2018.

[16] N. Dunkelberger, E. M. Schearer, and M. K. O'Malley, "A review of methods for achieving upper limb movement following spinal cord injury through hybrid muscle stimulation and robotic assistance," *Experim. Neurol.*, vol. 328, Jun. 2020, Art. no. 113274.

[17] M. O. Ibitoye, N. A. Hamzaid, M. Hayashibe, N. Hasnan, and G. M. Davis, "Restoring prolonged standing via functional electrical stimulation after spinal cord injury: A systematic review of control strategies," *Biomed. Signal Process. Control*, vol. 49, pp. 34–47,Mar. 2019.

[18] L. M. Dominguez, J. A. Mercado-Gutiérrez, J. Gutiérrez-Martínez, M. A. N. Gaona, and J. R. J. Alaniz, "Results of a survey applied to potential users of a functional electrical stimulation device and its use to design a user interface based on IEC 62366 and IEC 62304 standards," in *Proc. Congreso Nacional de Ingeniería Biomédica*, 2025, pp. 113–121.

[19] R. Mazzone, "Cycling induced by functional electrical stimulation: User experience evaluation and long-term performances assessment," Master's thesis, Dept. Electron., Inf. Bioeng., Politecnico di Milano, Milan, Italy, 2021.

[20] B. Moineau, M. Myers, S. S. Ali, M. R. Popovic, and S. L. Hitzig, "End-user and clinician perspectives on the viability of wearable functional electrical stimulation garments after stroke and spinal cord injury," *Disab. Rehabil., Assistive Technol.*, vol. 16, no. 3, pp. 241–250,Apr. 2021.

[21] Y. Pei, M. Tobita, B. Dirlikov, D. Arnold, C. Tefertiller, and A. Gorgey, "Consumer views of functional electrical stimulation and robotic exoskeleton in SCI rehabilitation: A mini review," *Artif. Organs*, vol. 49, no. 5, pp. 729–748, May 2025.

[22] E. Heald, K. Kilgore, R. Hart, C. Moss, and P. H. Peckham, "Myoelectric signal from below the level of spinal cord injury as a command source for an implanted upper extremity neuroprosthesis–a case report," *J. NeuroEngineering Rehabil.*, vol. 16, no. 1, pp. 1–6, Dec. 2019.

[23] M. Milosevic et al., "Why brain-controlled neuroprosthetics matter: Mechanisms underlying electrical stimulation of muscles and nerves in rehabilitation," *Biomed. Eng. OnLine*, vol. 19, no. 1, pp. 1–30,Dec. 2020.

[24] M. K. Buczak, J. M. Zollinger, A. Alsaleem, R. Imburgia, J. Rosenbluth, and J. A. George, "Intuitive, myoelectric control of adaptive sports equipment for individuals with tetraplegia," in *Proc. Int. Conf. Rehabil. Robot. (ICORR)*, Sep. 2023, pp. 1–6.

[25] M. K. Buczak et al., "Predicting motor intent from residual neck muscle activity in individuals with neck weakness from ALS," in *Proc. 47th Annu. Int. Conf. IEEE Eng. Med. Biol. Soc. (EMBC)*, Jul. 2025, pp. 1–6.

[26] T. C. Hansen, T. N. Tully, V. John Mathews, and D. J. Warren, "A multimodal assistive-robotic-arm control system to increase independence after tetraplegia," *IEEE Trans. Neural Syst. Rehabil. Eng.*, vol. 32, pp. 2124–2133, 2024.

[27] J. K. Muguro et al., "Development of surface EMG game control interface for persons with upper limb functional impairments," *Signals*, vol. 2, no. 4, pp. 834–851, Nov. 2021.

[28] K. M. Cole, M. K. Buczak, H. Zhang, and J. A. George, "A low-profile high-density electromyography neckband for recording neck muscle activity," in *Proc. 47th Annu. Int. Conf. IEEE Eng. Med. Biol. Soc. (EMBC)*, Jul. 2025, pp. 1–5.

[29] M. R. Williams and R. F. Kirsch, "Evaluation of head orientation and neck muscle EMG signals as three-dimensional command sources," *J. NeuroEngineering Rehabil.*, vol. 12, no. 1, p. 25, 2015.

[30] M. R. Williams and R. F. Kirsch, "Evaluation of head orientation and neck muscle EMG signals as command inputs to a human–computer interface for individuals with high tetraplegia," *IEEE Trans. Neural Syst. Rehabil. Eng.*, vol. 16, no. 5, pp. 485–496, Oct. 2008.

[31] T. Schauer, "Sensing motion and muscle activity for feedback control of functional electrical stimulation: Ten years of experience in Berlin," *Annu. Rev. Control*, vol. 44, pp. 355–374, Oct. 2017.

[32] G. Rolandino, M. Gagliardi, T. Martins, G. L. Cerone, B. Andrews, and J. J. FitzGerald, "Developing RPC-Net: Leveraging high-density electromyography and machine learning for improved hand position estimation," *IEEE Trans. Biomed. Eng.*, vol. 71, no. 5, pp. 1617–1627, May 2024.

[33] G. Rolandino, C. Zangrandi, T. Vieira, G. L. Cerone, B. Andrews, and J. J. FitzGerald, "HDE-array: Development and validation of a new dry electrode array design to acquire HD-sEMG for hand position estimation," *IEEE Trans. Neural Syst. Rehabil. Eng.*, vol. 32, pp. 4004–4013, 2024.

[34] G. Rolandino et al., "Performance of a ML-based 3-dof kinematic model in estimating hand position from high-density EMG," presented at the IFESS Conf., Sep. 2024.

[35] G. Rolandino, L. Lion, T. Vieira, I. Havoutis, B. Andrews, and J. J. FitzGerald, "Artificial neural networks for HD-sEMG-based hand position estimation: Addressing inter- and intra-subject variability," *J. NeuroEngineering Rehabil.*, to be published.

[36] G. Rolandino, G. Parisi, T. Vieira, I. Havoutis, B. Andrews, and J. J. FitzGerald, "Real-time hand kinematic estimation with hd-semg and artificial neural networks: Feasibility and effects of multi-subject training and visual feedback," submitted for publication.

[37] G. Rolandino et al., "Rpc-Net dataset. Simultaneous hd-semg recordings on the forearm and angles of a 29-dof hand kinematic model," Zenodo, Nov. 2024, doi: 10.5281/zenodo.14246378.

[38] G. L. Cerone, A. Botter, and M. Gazzoni, "A modular, smart, and wearable system for high density sEMG detection," *IEEE Trans. Biomed. Eng.*, vol. 66, no. 12, pp. 3371–3380, Dec. 2019.

[39] G. L. Cerone, A. Botter, T. Vieira, and M. Gazzoni, "Design and characterization of a textile electrode system for the detection of high-density sEMG," *IEEE Trans. Neural Syst. Rehabil. Eng.*, vol. 29, pp. 1110–1119, 2021, doi: 10.1109/TNSRE.2021.3086860.

[40] J. Wang, L. Bi, and W. Fei, "EEG-based motor BCIs for upper limb movement: Current techniques and future insights," *IEEE Trans. Neural Syst. Rehabil. Eng.*, vol. 31, pp. 4413–4427, 2023.

[41] S. M. Sarhan, M. Z. Al-Faiz, and A. M. Takhakh, "A review on EMG/EEG based control scheme of upper limb rehabilitation robots for stroke patients," *Heliyon*, vol. 9, no. 8, Aug. 2023, Art. no. e18308.

[42] S. Pancholi, A. Giri, A. Jain, L. Kumar, and S. Roy, "Source aware deep learning framework for hand kinematic reconstruction using EEG signal," *IEEE Trans. Cybern.*, vol. 53, no. 7, pp. 4094–4106,Jul. 2023.

[43] V. Mondini, A.-I. Sburlea, and G. R. Müller-Putz, "Towards unlocking motor control in spinal cord injured by applying an online EEG-based framework to decode motor intention, trajectory and error processing," *Sci. Rep.*, vol. 14, no. 1, p. 4714, Feb. 2024.

[44] S. M. Hosseini and V. Shalchyan, "Continuous decoding of hand movement from EEG signals using phase-based connectivity features," *Frontiers Human Neurosci.*, vol. 16, Jun. 2022, Art. no. 901285.

[45] M. Degirmenci, Y. K. Yuce, M. Perc, and Y. Isler, "EEG-based finger movement classification with intrinsic time-scale decomposition," *Frontiers Human Neurosci.*, vol. 18, Mar. 2024, Art. no. 1362135.

[46] Y. Ding, C. Udompanyawit, Y. Zhang, and B. He, "EEG-based brain–computer interface enables real-time robotic hand control at individual finger level," *Nature Commun.*, vol. 16, no. 1, pp. 1–20, Jun. 2025.

[47] D. Pei and R. Vinjamuri, "Decoding and generating synergy-based hand movements using electroencephalography during motor execution and motor imagery," *Biomed. Eng. Adv.*, vol. 9, Jun. 2025, Art. no. 100152.

[48] A. Richards, "University of Oxford advanced research computing," Zenodo, 2015, doi: 10.5281/zenodo.22558.